

Topological Horseshoes of Traveling Waves for a Fast-Slow Predator-Prey System

Marcio Gameiro

School of Mathematics, Georgia Institute of Technology,
Atlanta, Georgia, 30332, USA, gameiro@math.gatech.edu

Tomáš Gedeon

Department of Mathematical Sciences, Montana State University,
Bozeman, Montana, 59717, USA, gedeon@math.montana.edu

William Kalies

Department of Mathematical Sciences, Florida Atlantic University,
Boca Raton, Florida, 33431, USA, wkalties@fau.edu

Hiroshi Kokubu

Department of Mathematics, Kyoto University,
Kyoto, 606-8502, Japan, kokubu@math.kyoto-u.ac.jp

Konstantin Mischaikow

School of Mathematics, Georgia Institute of Technology,
Atlanta, Georgia, 30332, USA, mischaik@math.gatech.edu

Hiroe Oka

Department of Applied Mathematics and Informatics, Ryukoku University,
Seta, Otsu, 520-2194, Japan, oka@rins.ryukoku.ac.jp

October 19, 2005

Abstract

We show the existence of a set of periodic traveling waves in a system of two scalar reaction diffusion equations, which is in one-to-one correspondence with a full shift on two symbols. We use a novel combination of rigorous numerical computations and the topological techniques of the Conley index theory. This approach is quite general, and this paper is intended as a demonstration of its usefulness and applicability.

On the occasion of Pavol Brunovský's 70th Birthday.

1 Introduction

Nonlinear problems with two different time scales are often modeled by singularly perturbed ODEs called fast-slow systems, which often display interesting phenomena including periodic, heteroclinic or chaotic dynamics. Analytic and geometric methods have been successfully applied to study dynamics in fast-slow systems, provided certain properties are known, such as the basic structure of the fast and slow subsystems, hyperbolicity and transversality of relevant invariant manifolds, etc. See [5] for a survey of geometric singular perturbation theory. In practice, however, it is not always possible to verify these crucial properties by analytical methods.

In this paper, we illustrate how the topological method developed in [4] combined with rigorous numerical computation can be used to verify properties of fast-slow systems which are enough to prove the existence of periodic, heteroclinic, and chaotic solutions. As such we assume the reader is familiar with the notation and results in [4]. Unfortunately the level of abstraction in [4] can obscure the essential topological ideas underlying the method. Therefore in this paper we formulate concrete geometric hypothesis the numerical verification of which leads to the desired existence results.

The particular example considered in this paper is motivated by the work of Gardner and Smoller [3] on the existence of periodic traveling waves for a system of reaction diffusion equations of the form

$$\begin{aligned}\epsilon u_t &= \epsilon^2 u_{xx} + u f(u, v) \\ v_t &= v_{xx} + v g(u, v)\end{aligned}\tag{1.1}$$

where u and v are population densities of a prey and a predator species and $\epsilon > 0$ is small. They also assume that $\frac{\partial f}{\partial v} < 0$, $\frac{\partial g}{\partial u} > 0$, and that the zero

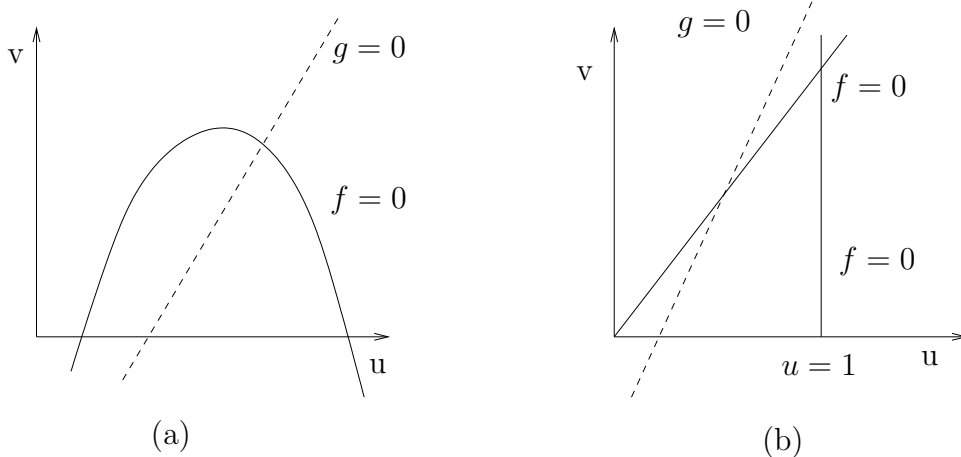


Figure 1: (a) General shape of the zero sets for the functions f and g in [3]. (b) Zero sets for the particular problem (1.3) considered in this paper. The v -axis and the right branch of $f = 0$ are branches of the slow manifolds M_1 and M_2 , respectively.

sets of f and g are as indicated in Figure 1. Choosing the traveling wave coordinate $\xi = (x - \theta t)/\epsilon$, the system (1.1) reduces to the fast-slow system

$$\begin{aligned}
 \dot{u} &= w \\
 \dot{w} &= -\theta w - u f(u, v) \\
 \dot{v} &= \epsilon z \\
 \dot{z} &= -\epsilon(\theta z + v g(u, v))
 \end{aligned} \tag{1.2}$$

where the derivatives are taken with respect to ξ .

Under the above, fairly general hypotheses on f and g and using the Conley index, Gardner and Smoller proved the existence of a periodic solution to (1.2) for $\epsilon > 0$, but sufficiently small. In this paper we consider a simplification of this problem, but using more sophisticated index techniques developed in [4] we prove the existence of not only periodic orbits but also a set of infinitely many bounded trajectories which are encoded by symbolic sequences. In particular, we define

$$\begin{aligned}
 f(u, v) &:= (1 - u)(u - v) \\
 g(u, v) &:= au - b - v
 \end{aligned} \tag{1.3}$$

and set $\theta = \pm 0.25$, $a = 1.65$, and $b = 0.25$. Our justification for considering this simplified set of equations is that it provides us with an easily under-

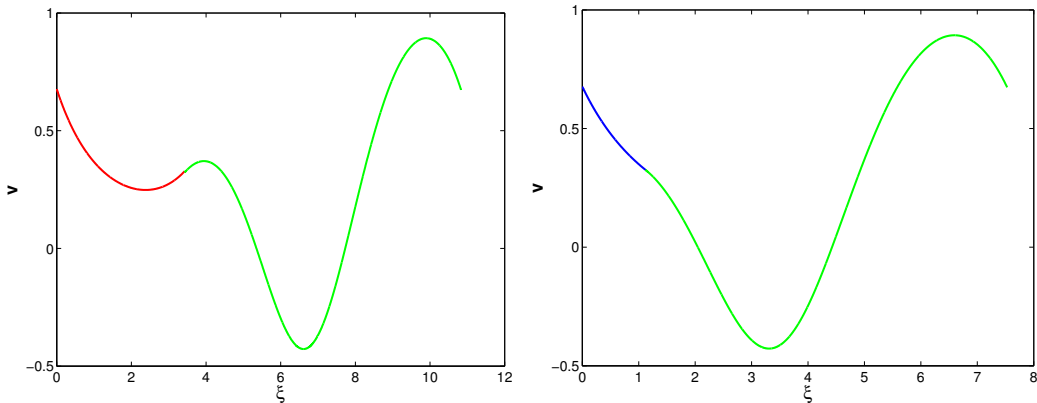


Figure 2: Plot of the two primitive periodic solutions to (1.2) for the particular choice of nonlinearities (1.3) with $\theta = -0.25$, $a = 1.65$, and $b = 0.25$.

stood system in which to demonstrate that these new index techniques can be combined in a straightforward manner with computational techniques to provide rigorous results about the dynamics of systems with two time scales. With regard to the methods, to a large extent the particular choices of θ , a , and b are arbitrary, though obviously the particular form of the dynamics depends on these parameters.

Theorem 1.1 *Consider (1.1) for the particular choice of nonlinearities (1.3), where $a = 1.65$, and $b = 0.25$. For $\epsilon > 0$ sufficiently small there exist two periodic traveling wave solutions with wave speed $\theta = -0.25$ whose profiles with respect to the v -variable are indicated in Figure 2.*

Theorem 1.2 *Consider (1.1) for the particular choice of nonlinearities (1.3), where $a = 1.65$, and $b = 0.25$. For $\epsilon > 0$ sufficiently small there exist two periodic traveling wave solutions with wave speed $\theta = 0.25$ whose profiles with respect to the v -variable are indicated in Figure 3.*

In what follows we only discuss the case $\theta = -0.25$. All the computations for $\theta = 0.25$ have been performed and show that this case can be treated in a similar manner as for $\theta = -0.25$. The proof of Theorem 1.1 is provided in Sections 2 and 3. In particular, in Section 2 we consider the *fast system* which is obtained by setting $\epsilon = 0$,

$$\begin{cases} \dot{u} = w \\ \dot{w} = -\theta w - u(1-u)(u-v). \end{cases} \quad (1.4)$$

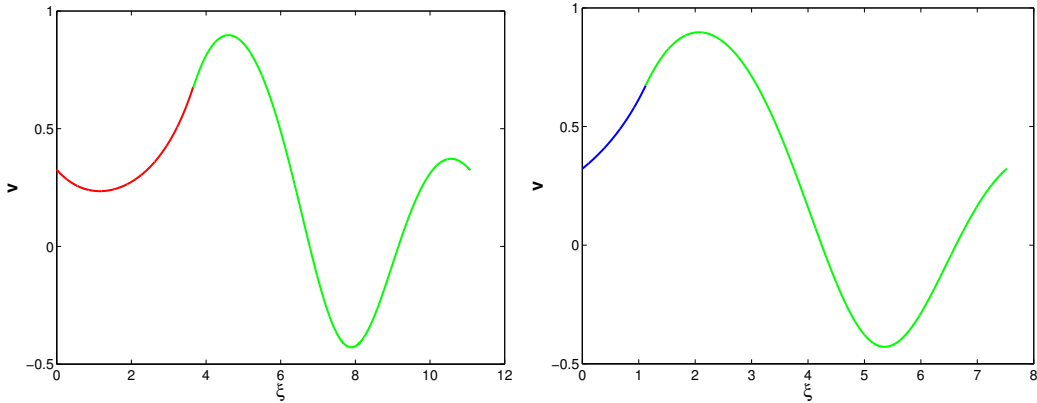


Figure 3: Plot of the two primitive periodic solutions to (1.2) for the particular choice of nonlinearities (1.3) with $\theta = 0.25$, $a = 1.65$, and $b = 0.25$.

We use numerical methods to find an isolating block for this system and to obtain bounds on the unstable manifolds of an equilibrium at different values of v .¹ As Theorem 2.1 indicates this is sufficient information to compute the associated topological transition matrix.

In Section 3 we consider the *slow system* which is obtained by rescaling time and restricting to the slow manifolds defined by $u = 0$ or $u = 1$,

$$\begin{cases} v' = z \\ z' = -\theta z - v(au - b - v) \end{cases} \quad u \in \{0, 1\}. \quad (1.5)$$

In this case we use numerics to obtain bounds for finite time trajectories for several points and check that they satisfy certain geometric constraints. In combination with the results of Section 2, Theorem 1.1 follows from [4, Theorem 1.6].

In Section 4, we prove Theorem 4.1 that allows us to extend Theorem 1.1 to the following result.

Theorem 1.3 *Consider (1.1) for the particular choice of nonlinearities (1.3), where $a = 1.65$, and $b = 0.25$. For $\epsilon > 0$ sufficiently small there exists a full*

¹In principle, for this particular problem this set could be obtained analytically. However an important goal of this paper is to demonstrate that currently available numerical methods can be combined with the topological tools of [4] to prove results for these two-time scale problems.

two-shift of traveling wave solutions with wave speed $\theta = -0.25$. The profiles with respect to the v -variable of these solutions are well approximated by arbitrary concatenations of the profiles indicated in Figure 2.

As we mentioned above, a similar extension of Theorem 1.2 applies to the case of $\theta = 0.25$.

In the context of fast-slow systems, the existence of various types of dynamics including chaotic solutions has already been proven and/or discussed by different approaches, see [6] and references therein.

Though the results of this paper are obtained by a careful interweaving of numerical and topological methods, for the sake of clarity in Sections 2 and 3 we treat the numerical results as if they had been obtained by rigorous analytical methods. The justification for the use of the numerical results is postponed to Section 5.

2 Fast Dynamics

In this section we discuss constructions involving the fast system (1.4). All these constructions have been performed numerically and the details of these computations are described in Section 5. For relevant definitions of these constructions we refer the reader to [4]. We have two basic goals in this section. The first is to construct a box, or rather a series of boxes, which are the sets possibly containing a heteroclinic solution between equilibrium points. Such a heteroclinic solution in the fast system, if it exists, corresponds to an inner layer of the periodic solutions of the entire fast-slow system. The second goal is to compute a particular entry in the topological transition matrix which, when nontrivial, indicates that such a heteroclinic solution does exist in the box. It will be more convenient to reverse the order and compute first the topological transition matrix.

Our general setting is a two-parameter family of differential equations

$$\dot{x} = h(x, \lambda), \quad x \in \mathbb{R}^2, \quad \lambda \in \Lambda, \quad (2.1)$$

which generates a flow $\psi_\lambda : \mathbb{R} \times \mathbb{R}^2 \rightarrow \mathbb{R}^2$, where $\Lambda \subset \mathbb{R}^2$. In our case the fast system (1.4) nominally generates such a two-parameter family of flows $\psi_{(v,z)}$, where v, z are parameters corresponding to the slow variables. However it is clear from the form of the equations that ψ depends only on the parameter v and thus we will often identify $\lambda = v$ in what follows.

Given a compact set $X \subset \mathbb{R}^2$, the *immediate exit set* and *immediate entrance set* of X under the flow ψ_λ are defined respectively as

$$\begin{aligned} X_\lambda^- &:= \{x \in \partial X \mid \psi_\lambda((0, t), x) \not\subset X \ \forall t > 0\} \quad \text{and} \\ X_\lambda^+ &:= \{x \in \partial X \mid \psi_\lambda((t, 0), x) \not\subset X \ \forall t < 0\}. \end{aligned}$$

In what follows we refer to a compact set X which is a simply-connected region in the (u, w) plane. This region is a result of a numerical computation and is identified as a list of edges (i.e. pairs of points) in \mathbb{R}^2 and the two-dimensional polygon they bound. The important property of X is that it allows one to compute the topological transition matrix. Therefore we formulate a set of assumptions on the set X which allows us to conclude that a off-diagonal entry, namely the $(2, 1)$ entry, of the topological transition matrix is an isomorphism. This is the key to the existence of heteroclinic solutions, namely inner layers, as shown in [4].

A1 X is homeomorphic to the closed unit disk.

A2 The immediate exit and immediate entrance sets of X are independent of λ for $\lambda \in \Lambda$, that is, there are sets $X^- = X_\lambda^-$ and $X^+ = X_\lambda^+$ for all $\lambda \in \Lambda$. Furthermore,

$$X^- = X_1^- \cup X_2^-$$

where X_i^- , $i = 1, 2$ are the compact connected components of X^- , and

$$\partial X = X^- \cup X^+.$$

A3 There exists a continuous Lyapunov function $V : X \times \Lambda \rightarrow \mathbb{R}$ with the property that

$$V(\psi_\lambda(t, x), \lambda) \leq V(x, \lambda)$$

for every $t > 0$ with equality if and only if x is an equilibrium point for (2.1).

A4 For each $\lambda \in \Lambda$ there exist exactly three hyperbolic equilibria $M_\lambda(i) \in X$, $i = 1, 2, 3$, of (2.1) which vary continuously as a function of λ . With regard to the Lyapunov function of **A3**, $i > j$ implies $V(M_\lambda(i), \lambda) > V(M_\lambda(j), \lambda)$. Furthermore, $M_\lambda(3)$ is a source and $M_\lambda(2)$ and $M_\lambda(1)$ are saddles.

The final assumption involves measuring the difference in the dynamics at λ_0 and λ_1 . Let $W^u(M_\lambda(2))$ denote the unstable manifold of $M_\lambda(2)$ under the flow ψ_λ . Let $W_{loc}^u(M_\lambda(2))$ denote the connected component of $W^u(M_\lambda(2)) \cap X$ which contains $M_\lambda(2)$.

A5 $W_{loc}^u(M_{\lambda_i}(2)) \cap X^- = \{x_{\lambda_i}^a, x_{\lambda_i}^b\}$ for $i = 0, 1$. Furthermore, $\{x_{\lambda_0}^a, x_{\lambda_0}^b\} \subset X_1^-$, while $x_{\lambda_1}^a \in X_1^-$ and $x_{\lambda_1}^b \in X_2^-$.

Recall that a *Morse decomposition*

$$\mathcal{M}(S) = \{M(p) \mid p \in (\mathcal{P}, >)\}$$

of an isolated invariant set S is a finite collection of disjoint compact invariant subsets $M(p)$, called *Morse sets*, indexed by a partially ordered set $(\mathcal{P}, >)$, with the property that: if $x \in S \setminus \bigcup_{p \in \mathcal{P}} M(p)$, then there exist $q > p$ such that the alpha limit set of x is contained in $M(q)$ and the omega limit set of x is contained in $M(p)$.

Theorem 2.1 *Given assumptions A1-A5, let $S_\lambda = \text{Inv}(X, \psi_\lambda)$. A Morse decomposition for S_λ is given by*

$$\mathcal{M}(S_\lambda) := \{M_\lambda(i) \mid i = 1, 2, 3\}$$

with admissible ordering $3 > 2 > 1$. Furthermore, S_λ and the Morse decomposition $\mathcal{M}(S_\lambda)$ continue over Λ . Let

$$T_{\lambda_1, \lambda_0} : CH^*(M_{\lambda_0}(1); \mathbb{Z}_2) \oplus CH^*(M_{\lambda_0}(2); \mathbb{Z}_2) \rightarrow CH^*(M_{\lambda_1}(1); \mathbb{Z}_2) \oplus CH^*(M_{\lambda_1}(2); \mathbb{Z}_2)$$

be the topological transition matrix defined over the interval Λ . Then,

$$T_{\lambda_1, \lambda_0}(2, 1) : CH^*(M_{\lambda_0}(1); \mathbb{Z}_2) \rightarrow CH^*(M_{\lambda_1}(2); \mathbb{Z}_2)$$

is an isomorphism.

Proof. Assumptions **A3** and **A4** guarantee that $\mathcal{M}(S_\lambda) := \{M_\lambda(i) \mid i = 1, 2, 3\}$ is a Morse decomposition for S_λ with admissible ordering $3 > 2 > 1$. Thus, $\{2, 1\}$ is an interval in the admissible ordering for all $\lambda \in \Lambda$. By Assumption **A5**,

$$M_{\lambda_i}(2, 1) = M_{\lambda_i}(2) \cup M_{\lambda_i}(1)$$

for $i = 0, 1$. Thus, the topological transition matrix T_{λ_1, λ_0} is defined, cf. [10].

It follows directly from assumptions **A2** and **A5** that $W_{loc}^u(M_{\lambda_0}(2))$ and $W_{loc}^u(M_{\lambda_1}(2))$ lie in different homotopy classes of the pointed topological space $(X/X^-, [X^-])$ which is the homotopy Conley index of S_λ . This implies that the connected simple systems at λ_0 and λ_1 differ, that is

$$I(M_{\lambda_0}(2, 1), \psi_{\lambda_0}) \not\cong I(M_{\lambda_1}(2, 1), \psi_{\lambda_1}).$$

Thus, by [10, Proposition 3.5] T_{λ_1, λ_0} is not the identity map. Since it must be lower triangular and we are using \mathbb{Z}_2 coefficients, the only option is $T_{\lambda_1, \lambda_0}(2, 1) = 1$. Hence, $T_{\lambda_1, \lambda_0}(2, 1)$ is an isomorphism. \square

We now show that Assumptions **A1-A5** are satisfied for equations (1.4).

Lemma 2.2 *Let X be the simply connected region defined in Figure 4. Then, Assumptions **A1** and **A2** are satisfied for the fast system (1.4) for $v \in \Lambda = [0.275, 0.7]$.*

Proof. Using interval arithmetic it was shown that the vector field associated with (1.4) is transverse to the boundary edges for all values of $v \in \Lambda = [0.275, 0.7]$ and there are no internal tangencies at a vertex. This implies that each boundary edge is either an element of X^- or of X^+ . Those boundary edges which belong to X^- are indicated in black (dashed) and those boundary edges which belong to X^+ are indicated in red (solid). Clearly X^- consists of two connected components, and this is confirmed in the numerical construction of X . The list of edges forming ∂X is shown in Table 1. \square

A straightforward calculation implies the following two lemmas.

Lemma 2.3 *The function $V : \mathbb{R}^2 \times \Lambda \rightarrow \mathbb{R}$ defined by*

$$V(u, w, v) = -\frac{w^2}{2} + u^2 \left(\frac{u^2}{4} - \frac{(1+v)u}{3} + \frac{v}{2} \right)$$

*satisfies **A3** for $\Lambda = [0.323, 0.326]$ and $\Lambda = [0.674, 0.677]$.*

Lemma 2.4 *For $v \in [0.323, 0.326] \cup [0.674, 0.677]$ the equilibria of (1.4) are $\{(0, 0), (v, 0), (1, 0)\}$. For $v \in [0.323, 0.326]$,*

$$M(3) = (v, 0), \quad M(2) = (0, 0), \quad M(1) = (1, 0).$$

For $v \in [0.674, 0.677]$,

$$M(3) = (v, 0), \quad M(2) = (1, 0), \quad M(1) = (0, 0).$$

*In both cases, **A4** is satisfied.*

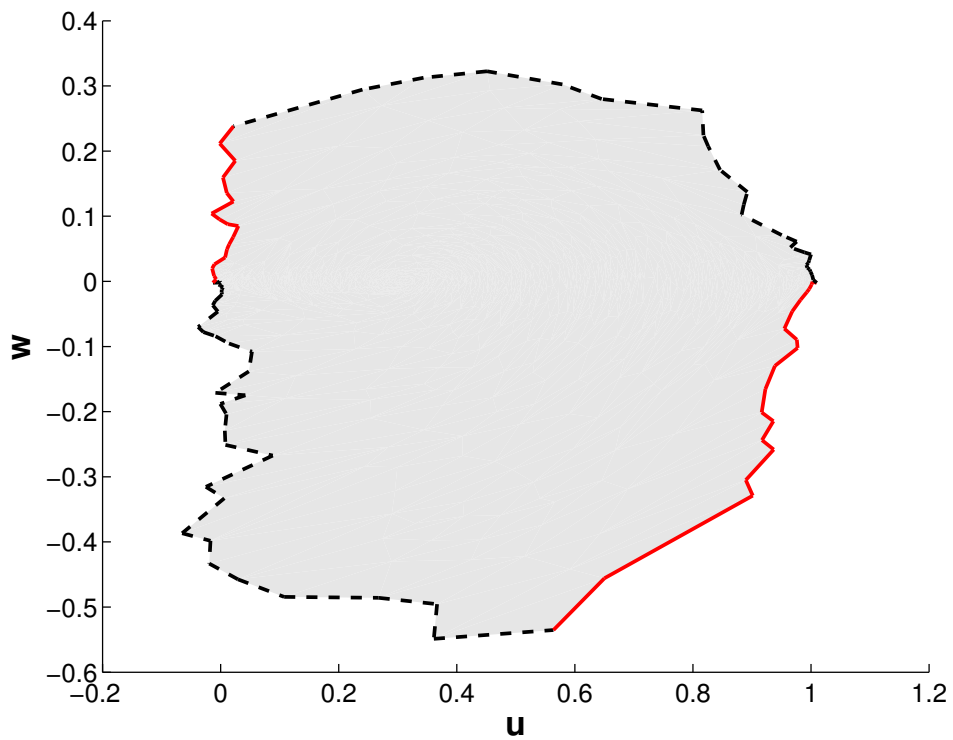


Figure 4: Isolating block X for (1.4) for all $v \in [0.275, 0.7]$. The exact list of vertices forming ∂X is in Table 1. The black (dashed) portion of ∂X is the immediate exit set, X^- , and red (solid) portion is the immediate entrance set, X^+ .

Lemma 2.5 Let $\Lambda = [v_0, v_1] = [0.323, 0.326]$ and for $i = 0, 1$ let

$$W_{loc}^u(M_{v_i}(2)) \cap X^- = \{x_{v_i}^a, x_{v_i}^b\}.$$

Then

$$\{x_{v_0}^a, x_{v_0}^b\} \subset X_1^-$$

and

$$x_{v_1}^a \in X_1^- \quad \text{and} \quad x_{v_1}^b \in X_2^-.$$

Proof. The lemma follows directly from Figure 5. The unstable manifolds in Figure 5 are rigorously computed. A detailed discussion of how these computations were performed can be found in Section 5. \square

In a similar manner the proof of the following lemma follows from Figure 6.

Lemma 2.6 Let $\Lambda = [v_0, v_1] = [0.674, 0.677]$ and for $i = 0, 1$ let $W_{loc}^u(M_{v_i}(2)) \cap X^- = \{x_{v_i}^a, x_{v_i}^b\}$. Then

$$x_{v_0}^a \in X_1^- \quad \text{and} \quad x_{v_0}^b \in X_2^-$$

and

$$\{x_{v_1}^a, x_{v_1}^b\} \subset X_1^-.$$

We now turn to the construction of boxes. Let

$$Y_l := (\mathbb{R} \times (-\infty, -\delta)) \cup ((\delta, 1 - \delta) \times (-\infty, 0)) \cup ((0.323 - \delta, 0.326 + \delta) \times [0, \delta])$$

and

$$Y_r := (\mathbb{R} \times (\delta, \infty)) \cup ((\delta, 1 - \delta) \times (0, \infty)) \cup ((0.674 - \delta, 0.677 + \delta) \times (-\delta, 0]).$$

Define X_l as the connected component of $X \setminus Y_l$ that contains the saddle equilibrium points, and similarly X_r as the connected component of $X \setminus Y_r$ containing the saddle equilibria. Observe that the sets $X \setminus Y_l$ and $X \setminus Y_r$ may not be connected but cannot have “holes” in any connected component, since X is homeomorphic to the unit disk by its construction and since Y_l and Y_r are simply connected unbounded domains. Thus, if δ is sufficiently small, X_l and X_r are well-defined and homeomorphic to the unit disk.

Let $\varphi_u : \mathbb{R} \times \mathbb{R}^2 \rightarrow \mathbb{R}^2$ be the slow flow on the associated slow manifold defined by (1.5) and $u \in \{0, 1\}$. For appropriate choice of z , let $Z(1, z) \subset [0.323, 0.326] \times \mathbb{R}$ denote the unique orbit segment of φ_1 that connects the point $(0.323, z)$ to the line $0.326 \times \mathbb{R}$.

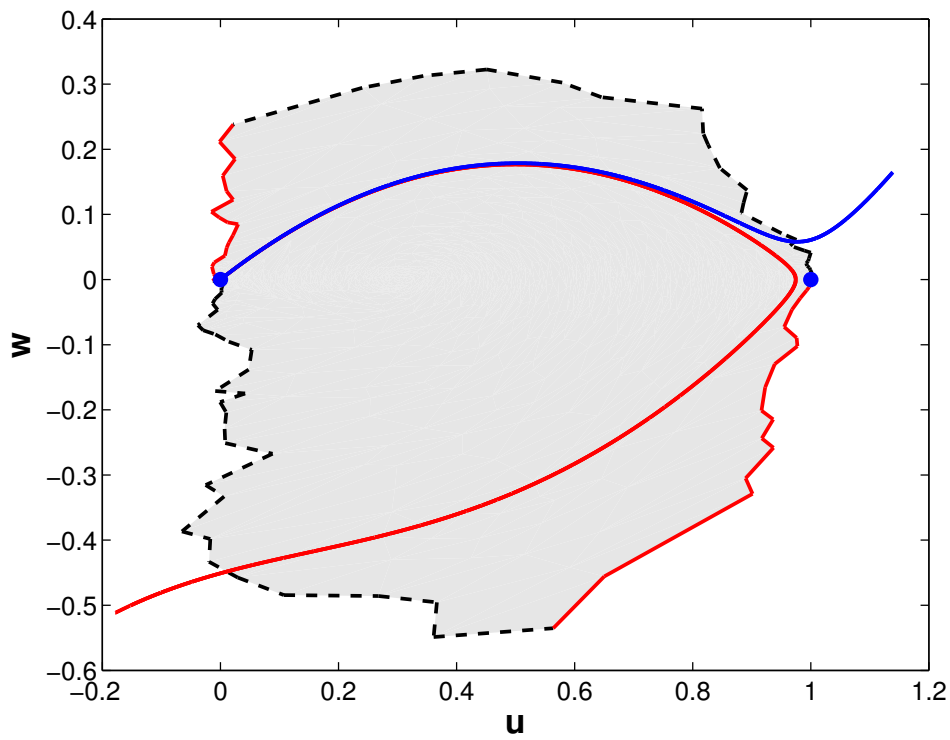


Figure 5: Unstable manifolds of the fixed point $(0,0)$ for (1.4). The red (bottom) curve correspond to $v = 0.323$ and the blue (top) curve to $v = 0.326$.

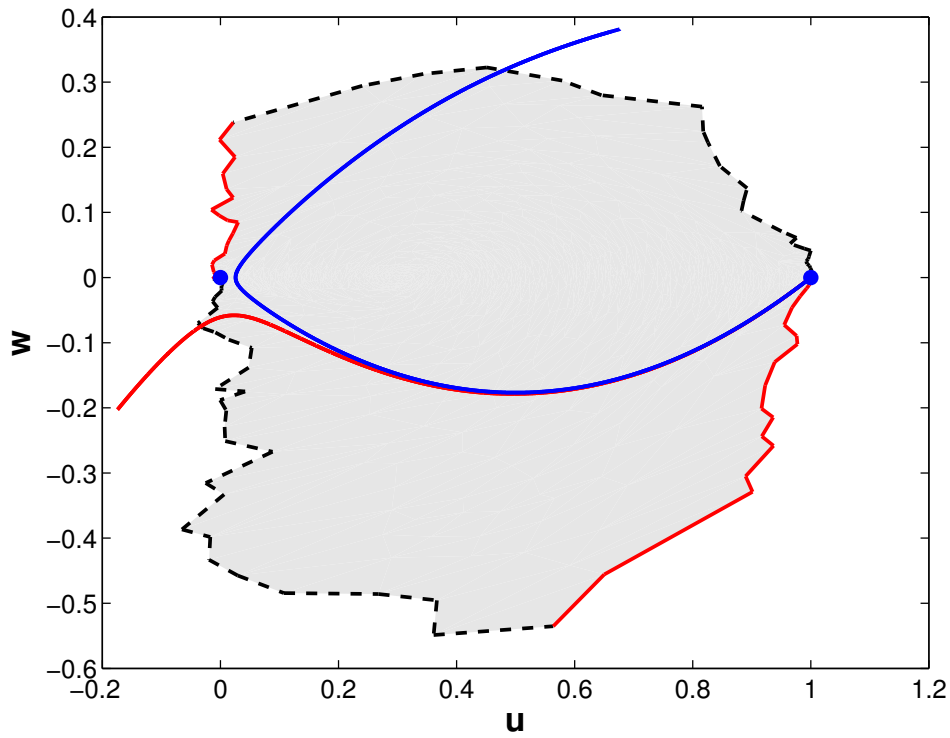


Figure 6: Unstable manifolds of the fixed point $(1, 0)$ for (1.4). The red (bottom) curve correspond to $v = 0.674$ and the blue (top) curve to $v = 0.677$.

Proposition 2.7 Choose $-\infty < z_* < z^* \leq -0.1$ and define $\mathcal{B} \subset \mathbb{R}^2$ to be the region bounded by the curves $0.323 \times \mathbb{R}$, $0.326 \times \mathbb{R}$, $Z(1, z_*)$, and $Z(1, z^*)$. Then, $\mathbf{B} := X_l \times \mathcal{B} \subset \mathbb{R}^4$ is a box.

Proof. The first step is to check that X_l is well defined. From the form of the vector field it is sufficient to check that $Z(1, -0.1)$ is defined. However, this follows from the Mean Value Theorem. It remains to check conditions (1)-(5) of [4, Definition 1.5].

(1) We need to show that \mathbf{B} is an isolating neighborhood for $\psi_{(v,z)}$ for all $(v, z) \in \mathcal{B}$. Observe that by Lemmas 2.3 and 2.4, for fixed $(v, z) \in \mathcal{B}$, $\text{Inv}(X_l, \psi_{(v,z)})$ consists of the equilibria $(0, 0)$ and $(1, 0)$ and possibly a connecting orbit from $(0, 0)$ to $(1, 0)$. Also, notice that for fixed (v, z) the vector field associated with the fast dynamics (1.4) is transverse to the boundary of X_l except near the equilibria $(0, 0)$, $(1, 0)$ and $(v, 0)$. For $\delta > 0$, but sufficiently small, we can use the Unstable Manifold Theorem to conclude that there are no internal tangencies of a connecting orbit from $(0, 0)$ to $(1, 0)$ near $(0, 0)$ and $(1, 0)$. Furthermore, given (u, w) in a sufficiently small neighborhood of $(v, 0)$ for $v \in [0.323, 0.326]$, $V(u, w, v) > V(0, 0, v)$ precluding the possibility of a $(0, 0)$ to $(1, 0)$ connecting orbit passing near $[0.323 - \delta, 0.326 + \delta] \times [0, \delta]$.

(2) This follows from Lemma 2.4 where $M(2) = (0, 0)$ and $M(1) = (1, 0)$.

(3) This is a triviality since $M(2)$ and $M(1)$ remain constant for all values of $(v, z) \in \mathcal{B}$.

(4) For $\mu > 0$ but sufficiently small, let $\mathcal{B}^0 = [0.323, 0.323 + \mu] \times \mathbb{R} \cap \mathcal{B}$ and $\mathcal{B}^0 = [0.326 - \mu, 0.326] \times \mathbb{R} \cap \mathcal{B}$. The result now follows from Lemma 2.6.

(5) By construction X_l is homeomorphic to a two-dimensional disk. \square

The proofs of the following two propositions are similar.

Proposition 2.8 Choose $0.1 \leq z_* < z^* < \infty$ and define $\mathcal{B} \subset \mathbb{R}^2$ to be the region bounded by the curves $0.323 \times \mathbb{R}$, $0.326 \times \mathbb{R}$, $Z(1, z_*)$, and $Z(1, z^*)$. Then, $\mathbf{B} := X_l \times \mathcal{B} \subset \mathbb{R}^4$ is a box.

For appropriate choice of z , let $Z(0, z) \subset [0.674, 0.677] \times \mathbb{R}$ denote the unique orbit segment of φ_0 that connects the point $(0.674, z)$ to the line $0.677 \times \mathbb{R}$.

Proposition 2.9 Choose $-\infty < z_* < z^* \leq -0.1$ and define $\mathcal{B} \subset \mathbb{R}^2$ to be the region bounded by the curves $0.674 \times \mathbb{R}$, $0.677 \times \mathbb{R}$, $Z(0, z_*)$, and $Z(0, z^*)$. Then, $\mathbf{B} := X_r \times \mathcal{B} \subset \mathbb{R}^4$ is a box.

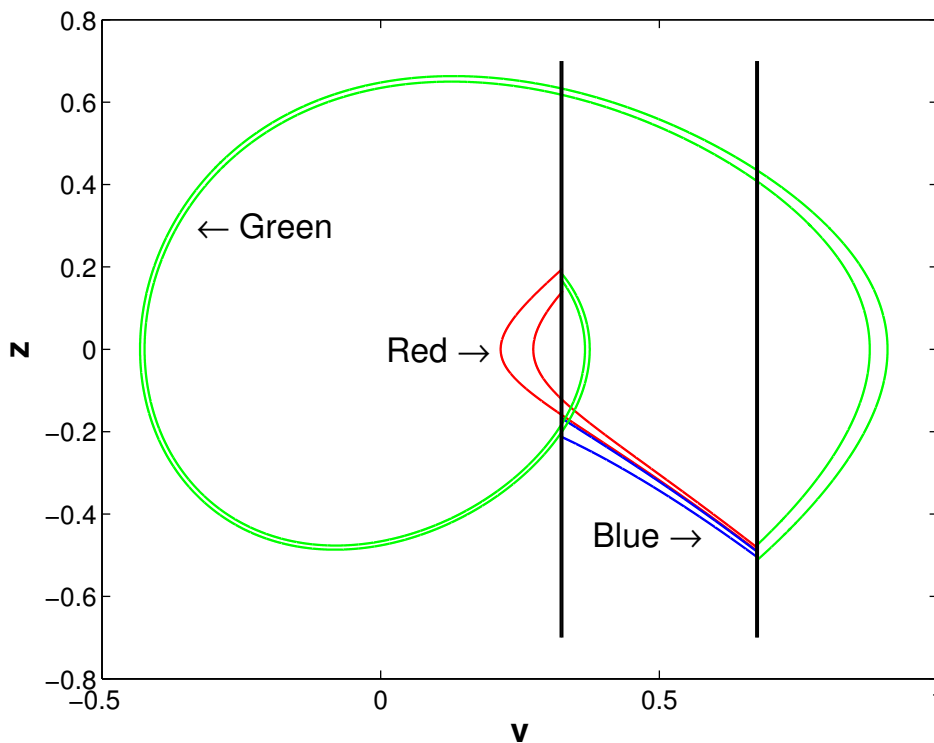


Figure 7: Orbits of (1.5). The blue and red curves are for $u = 0$ and the green curves are for $u = 1$. We refer to the regions between these curves as the blue, red, and green regions. The vertical black lines are the lines $v = 0.323$, $v = 0.326$, $v = 0.674$ and $v = 0.677$.

3 Slow dynamics

In this section we study the slow flows φ_0 and φ_1 given by (1.5) with $u = 0$ and $u = 1$, respectively. In order to compare these two flows we project them to flows ψ_0 and ψ_1 on the (v, z) space. The main data we use as input is depicted in Figure 7 with close-ups of regions of interest in Figure 8. All curves in these figures have been computed numerically and details of these computations can be found in Section 5. For the purposes of this section it is sufficient to assume that the red, green, and blue curves are flow lines of one of the flows ψ_0, ψ_1 .

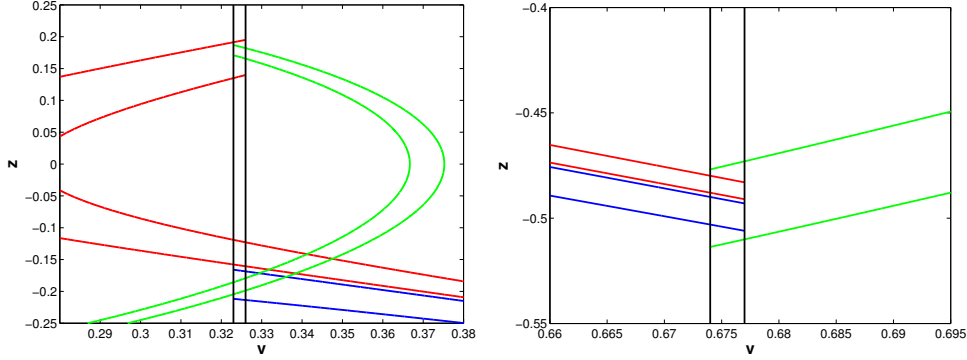


Figure 8: Close-ups of Figure 7 near the regions where the orbits “connect”.

In the following construction we refer to Figure 7. Let

$$\mathcal{R}_R := [0.323, 0.326] \times [0.1, 0.2] \quad \text{and} \quad \mathcal{R}_B := [0.323, 0.326] \times [-0.1, -0.4]$$

be two regions between the two black lines given by $v = 0.323$ and $v = 0.326$. Let

$$\mathcal{R}' := [0.674, 0.677] \times [-0.4, -0.6]$$

be a region between the two black lines given by $v = 0.674$ and $v = 0.677$. Further, we let

- \mathcal{E}_B be a ψ_0 flow box starting at some section $\Sigma_B \subset \{v = 0.677\}$ and ending at the black line $\{v = 0.323\}$;
- \mathcal{E}_R be a ψ_0 flow box starting at some section $\Sigma_R \subset \{v = 0.677\}$ and ending at the black line $\{v = 0.326\}$;
- \mathcal{E}'_R be a ψ_1 flow box starting at some section $\Sigma'_R \subset \{v = 0.323\}$ and ending at the black line $\{v = 0.674\}$;
- $\mathcal{E}'_B \subset \mathcal{E}'_R$ be a ψ_1 flow box starting at some section $\Sigma'_B \subset \{v = 0.326\}$ and ending at the black line $\{v = 0.674\}$.

The sections Σ_B and Σ_R are selected so that they lie strictly between the computed blue and red curves respectively. Also the sections Σ'_B and Σ'_R are selected so that they lie strictly between the computed green curves. These curves are computed using interval arithmetic and they enclose a true orbit

of the system. We choose these orbits as the boundaries of our sets, see Figure 7 and Figure 8.

The goal of this section is to verify conditions [4, **(H1)**-**(H4)**] and the conditions of [4, Definition 5.3]. We show in Theorem 3.2 that the following conditions **(B1)**-**(B6)** are sufficient for this purpose. These conditions relate to collections of the form $\{(\psi_i, \mathcal{E}_i, \mathcal{R}_i)\}_{i=0}^I$, where $\psi_i : \mathbb{R} \times \mathbb{R}^2 \rightarrow \mathbb{R}^2$ is a flow on \mathcal{E}_i and indices are cyclic, i.e $I + 1 = 0$.

- B1** The sets \mathcal{R}_i are homeomorphic to $J_i \times [a_i, b_i]$, where J_i is an interval.
- B2** For all i , the flow ψ_i is transverse to interval $J_{i+1} \times \{t_{i+1}\}$ for all $t_{i+1} \in [a_{i+1}, b_{i+1}]$, as well as to the interval $J_i \times \{t_i\}$ for all $t_i \in [a_i, b_i]$.
- B3** The flow ψ_i enters the set \mathcal{R}_j through $J_j \times \{a_j\}$ and leaves \mathcal{R}_j through the set $J_j \times \{b_j\}$, for $j = i, i + 1$.
- B4** The set \mathcal{E}_i has the form

$$\mathcal{E}_i = \bigcup_{z \in \Sigma_i} \varphi_i([0, T(z)], z)$$

where $\Sigma_i \subset J_{i+1} \times \{a_{i+1}\}$ is an interval and $T(z)$ is given by $\varphi(T(z), z) \in J_i \times \{a_i\}$.

- B5** $(\mathcal{E}_i \cap \mathcal{R}_{i-1}) \subsetneq (\mathcal{E}_{i-1} \cap \mathcal{R}_{i-1})$ for all i .

- B6** Flows ψ_{i+1} and ψ_i are transverse to each other in \mathcal{R}_i for all i .

We consider two regions: the union of the red and green regions and the union of the blue region with part of the green region in Figure 7. Note that these regions contain the primitive periodic orbits in Figure 2.

Theorem 3.1 *The collections*

$$\{(\psi_0, \mathcal{E}_R, \mathcal{R}_R), (\psi_1, \mathcal{E}'_R, \mathcal{R}')\} \text{ and } \{(\psi_0, \mathcal{E}_B, \mathcal{R}_B), (\psi_1, \mathcal{E}'_B, \mathcal{R}')\}$$

satisfy **(B1)**-**(B6)**.

Proof. For the first collection we set

$$\mathcal{E}_1 := \mathcal{E}'_R, \mathcal{R}_1 := \mathcal{R}', \mathcal{E}_0 := \mathcal{E}_R, \mathcal{R}_0 := \mathcal{R}_R.$$

For the second collection let

$$\mathcal{E}_1 := \mathcal{E}'_B, \mathcal{R}_1 := \mathcal{R}', \mathcal{E}_0 := \mathcal{E}_B, \mathcal{R}_0 := \mathcal{R}_B.$$

We will provide a detailed argument for the first collection and leave the analogous proof for the second collection for the reader. We set

$$a_1 := 0.323, b_1 := 0.326, a_2 := 0.677 \text{ and } b_2 := 0.674.$$

With this identification **(B1)** and **(B3)** follow immediately. The assumption **(B4)** follows from the construction of the sets \mathcal{E}_i , since the side boundaries are flow lines of the flow ψ_i , $i = 0, 1$. The assumption **(B5)** follows by inspection from Figure 8.

To verify **(B2)** we take a dot product of the vector fields (1.5)

$$(z, -\theta z + v(b+v) - av) \text{ and } (z, -\theta z + v(b+v)),$$

corresponding to ψ_1 and ψ_0 , respectively, with the normal $(1, 0)$ to the curves defined by constant v . In both cases this dot product is z , which is nonzero in \mathcal{R}_i with $i = 0, 1$.

To verify the transversality condition **(B6)** we take the dot product of the first vector field $(z, -\theta z + v(b+v))$ and the normal of the second vector field $(\theta z - v(b+v) + av, z)$. This dot product is

$$(z, -\theta z + v(b+v)) \cdot (\theta z - v(b+v) + av, z) = avz$$

which is nonzero in \mathcal{R}_i with $i = 0, 1$, since $v \neq 0$ in \mathcal{R}_i . □

Let Π be the projection onto slow variables $(u, w, v, z) \rightarrow (v, z)$. We have the following general theorem.

Theorem 3.2 *Consider a collection $\{(\psi_i, \mathcal{E}_i, \mathcal{R}_i)\}_{i=0}^I$ satisfying **(B1)**-**(B6)**. For any i , let*

$$\mathcal{B}_i := \mathcal{E}_i \cap \mathcal{R}_i \cap \mathcal{E}_{i-1}. \tag{3.1}$$

If $\mathcal{B}_i = \Pi(\mathbf{B}_i)$, namely the projection of a box \mathbf{B}_i , then the set $\bigcup_{i=1}^I E_i \cup \bigcup_{i=1}^I \mathbf{B}_i$ contains a periodic corridor. (Compare Propositions 2.7, 2.8 and 2.9.)

Proof. We need to verify [4, **(H1)**-**(H4)**] and the assumptions of [4, Definition 5.3]. The assumption **(H1)** is the same as (3.1), **(H2)** is **(B1)** and **(H3)** is **(B3)**. Assumption **(H4)** follows from the transversality assumption **(B6)**.

The first condition of [4, Definition 5.3] is the assumption that $\mathcal{B}_i = \Pi(\mathbf{B}_i)$ is a projection of a box. We set $\mathcal{B}_i^{\text{side}} := \text{cl}(\partial\mathcal{B}_i \setminus (\mathcal{R}_i \times \{a_i, b_i\}))$. Further, let $\mathcal{V}_i^- \subset \mathcal{E}_i$ be the collection of points z such that $\psi_i(t, z) \cap \mathcal{B}_i = \emptyset$, where we restrict the flow ψ_i to \mathcal{E}_i . These points will not enter the next set \mathcal{E}_{i-1} and will exit the collection $\bigcup_{i=1}^I \mathcal{E}_i$. Let $V_i^- \subset E_i^-$ with the property that $\mathcal{V}_i^- = \Pi(V_i^-)$. Notice that by assumption **(B5)**

$$\mathcal{E}_i^{\text{side}} \subset \mathcal{V}_i^- \quad (3.2)$$

where $\mathcal{E}_i^{\text{side}} := \bigcup_{z \in \partial\Sigma_i} \psi_i(T(z), z)$ is the side boundary of the set \mathcal{E}_i .

The second condition of [4, Definition 5.3] is

$$\mathcal{B}_i^{\text{side}} \setminus \mathcal{U}_i^{\text{side}} \subset \mathcal{V}_{i-1}^-.$$

To verify this condition it is enough to observe that by (3.1), **(B3)** and **(B5)** we have $\mathcal{B}_i^{\text{side}} \subset \mathcal{E}_{i-1}^{\text{side}}$. The result now follows from (3.2). Notice that we did not have to define the set $\mathcal{U}_i^{\text{side}}$ to obtain this result. For the definition of this set, the reader is referred to [4, after (5.2) and after Remark 5.2].

The next condition of [4, Definition 5.3] is

$$U_i^{\text{side}} \subset \text{int}_{U_i} V_i^+ \cup \text{int}_{U_i} V_i^-.$$

The set V_i^+ is the set of those points in E_i whose projections to \mathcal{E}_i never enter \mathcal{E}_{i-1} . By **(B5)** $V_i^+ = \emptyset$ for all i . The set

$$U_i^{\text{side}} \subset E_i^{\text{side}}$$

where $\mathcal{E}_i^{\text{side}} = \Pi(E_i^{\text{side}})$. Thus we get by (3.2) and **(B5)**

$$U_i^{\text{side}} \subset E_i^{\text{side}} \subset V_i^- \subset \text{int}_{U_i} V_i^- = \text{int}_{U_i} V_i^+ \cup \text{int}_{U_i} V_i^-.$$

This finishes verification of the second condition of [4, Definition 5.3].

The last two assumptions we need to verify is the existence of homotopy equivalences of pairs (see [4, Definition 5.3])

$$\begin{aligned} h_0 : (\mathcal{B}_i^{\text{in}}, \mathcal{B}_i^{\text{in}} \cap \mathcal{V}_{i-1}^-) &\hookrightarrow (\tilde{\mathcal{U}}_i^{\text{out}}, \tilde{\mathcal{U}}_i^{\text{out}} \cap \mathcal{V}_i^-), \\ h_1 : (\mathcal{B}_i^{\text{out}}, \mathcal{B}_i^{\text{out}} \cap \mathcal{V}_{i-1}^-) &\hookrightarrow (\tilde{\mathcal{U}}_{i-1}^{\text{in}}, \tilde{\mathcal{U}}_{i-1}^{\text{in}} \cap \mathcal{V}_{i-1}^-). \end{aligned}$$

It follows immediately from the definition of these sets in [4] that in our setting these are equivalent to

$$\begin{aligned} h_0 &: (\mathcal{B}_i^{a_i}, \mathcal{B}_i^{a_i} \cap \mathcal{V}_{i-1}^-) \hookrightarrow (\mathcal{E}_i^{a_i}, \mathcal{E}_i^{a_i} \cap \mathcal{V}_i^-), \\ h_1 &: (\mathcal{B}_i^{b_i}, \mathcal{B}_i^{b_i} \cap \mathcal{V}_{i-1}^-) \hookrightarrow (\mathcal{E}_{i-1}^{b_i}, \mathcal{E}_{i-1}^{b_i} \cap \mathcal{V}_{i-1}^-) \end{aligned} \quad (3.3)$$

where $Y^\lambda := Y \cap (\mathcal{R}_i \times \{\lambda\})$ for $Y = \mathcal{B}_i, \mathcal{E}_i, \mathcal{E}_{i-1}$. Observe that by (3.2) $(\mathcal{B}_i^{a_i}, \mathcal{B}_i^{a_i} \cap \mathcal{V}_{i-1}^-) \cong (\mathcal{B}_i^{a_i}, \partial \mathcal{B}_i^{a_i})$ and that $\mathcal{B}_i^{a_i}$ is an interval. The set $\mathcal{E}_i^{a_i}$ is an interval with $\mathcal{B}_i^{a_i} \subsetneq \mathcal{E}_i^{a_i}$ and $\mathcal{E}_i^{a_i} \setminus \mathcal{B}_i^{a_i} \subset \mathcal{V}_i^-$. Thus a deformation retract of $\mathcal{E}_i^{a_i}$ to $\mathcal{B}_i^{a_i}$ induces the desired homotopy equivalence h_0 . Similarly, a deformation retract of the interval $\mathcal{E}_{i-1}^{b_i}$ onto its proper subinterval $\mathcal{B}_i^{b_i}$ induces the homotopy equivalence h_1 . \square

Corollary 3.3 *Consider the collections*

$$\{(\psi_0, \mathcal{E}_B, \mathcal{R}_B), (\psi_1, \mathcal{E}'_B, \mathcal{R}')\} \text{ and } \{(\psi_0, \mathcal{E}_R, \mathcal{R}_R), (\psi_1, \mathcal{E}'_R, \mathcal{R}')\}.$$

For the first collection let

$$\mathcal{B}_B := \mathcal{E}_B \cap \mathcal{R}_B \cap \mathcal{E}'_B, \quad \mathcal{B}'_B := \mathcal{E}'_B \cap \mathcal{R}' \cap \mathcal{E}_B$$

and for the second collection let

$$\mathcal{B}_R := \mathcal{E}_R \cap \mathcal{R}_R \cap \mathcal{E}'_R, \quad \mathcal{B}'_R := \mathcal{E}'_R \cap \mathcal{R}' \cap \mathcal{E}_R.$$

Then there are periodic corridors

$$\mathbf{PC}_B \subset E_B \cup \mathbf{B}_B \cup E'_B \cup \mathbf{B}'_B \text{ and } \mathbf{PC}_R \subset E_R \cup \mathbf{B}_R \cup E'_R \cup \mathbf{B}'_R,$$

where \mathbf{B}_i and \mathbf{B}'_i , $i = R, B$ are boxes with $\Pi(\mathbf{B}_i) = \mathcal{B}_i$ and $\Pi(\mathbf{B}'_i) = \mathcal{B}'_i$.

Proof. By Propositions 2.7, 2.8 and 2.9, the sets $\mathcal{B}_i, \mathcal{B}'_i$ with $i = R, B$ are projections of boxes. By Theorem 3.1 these collections satisfy **(B1)**-**(B6)**. The result now follows from Theorem 3.2. \square

Corollary 3.4 *For all sufficiently small $\epsilon > 0$ there are two periodic solutions Γ_B and Γ_R of the system (1.2), whose projections to slow variables lie in $\mathcal{E}_B \cup \mathcal{E}'_B$ and $\mathcal{E}_R \cup \mathcal{E}'_R$ respectively.*

Proof. Corollary 3.3 verifies the existence of a periodic corridor containing boxes $\mathbf{B}_i, \mathbf{B}'_i$ with $i = R, B$, and Theorem 2.1 guarantees that the relevant entries of the topological transition matrices are all isomorphisms. Thus, [4, Theorem 1.6], there exist the desired periodic solutions for sufficiently small $\epsilon > 0$. \square

4 Topological Horseshoes of Traveling Waves

Theorem 4.1 *For a sufficiently small $\varepsilon > 0$ and any symbolic sequence $\sigma \in \{\mathbf{R}, \mathbf{B}\}^{\mathbb{Z}}$, the system (1.2) has a solution*

$$\mathbf{x}_\varepsilon^\sigma(t) = (u_\varepsilon^\sigma(t), v_\varepsilon^\sigma(t), w_\varepsilon^\sigma(t), z_\varepsilon^\sigma(t))$$

which satisfies the following condition: there exists a sequence of intervals $[t_i^-, t_i^+]$ for $i \in \mathbb{Z}$ such that, for all $i \in \mathbb{Z}$,

$$\Pi(\mathbf{x}_\varepsilon^\sigma([t_i^-, t_i^+])) \subset E_{\sigma_i} \quad \text{and} \quad \Pi(\mathbf{x}_\varepsilon^\sigma([t_i^+, t_{i+1}^-])) \subset E'_{\sigma_i}.$$

Proof. Recall that we have constructed the sets $E_{\mathbf{R}}$, $E_{\mathbf{B}}$, and $E'_{\mathbf{R}}$, $E'_{\mathbf{B}}$, as well as the boxes $\mathbf{B}_{\mathbf{R}}$, $\mathbf{B}_{\mathbf{B}}$, and $\mathbf{B}'_{\mathbf{R}}$, $\mathbf{B}'_{\mathbf{B}}$. Note $E'_{\mathbf{B}} \subset E'_{\mathbf{R}}$. We have showed in Corollary 3.3 that there are periodic corridors

$$\mathbf{PC}_{\mathbf{R}} \subset E_{\mathbf{R}} \cup \mathbf{B}_{\mathbf{R}} \cup E'_{\mathbf{R}} \cup \mathbf{B}'_{\mathbf{R}}$$

and

$$\mathbf{PC}_{\mathbf{B}} \subset E_{\mathbf{B}} \cup \mathbf{B}_{\mathbf{B}} \cup E'_{\mathbf{B}} \cup \mathbf{B}'_{\mathbf{B}}$$

that contain the basic periodic orbits $\Gamma_{\mathbf{R}}$ and $\Gamma_{\mathbf{B}}$, respectively (Corollary 3.4). Using the results in [4], we can then construct, for each \mathbf{PC}_a with $a = \mathbf{R}, \mathbf{B}$, a singular isolating neighborhood \mathbf{N}_a ([4, Lemma 5.8]) and a singular index pair $(\bar{\mathbf{N}}_a, \bar{\mathbf{L}}_a)$ ([4, Proposition 5.12]). Moreover, from the construction of these sets given in [4], we have that

- (1) there exists $\bar{\varepsilon} > 0$ such that, for any $0 < \varepsilon < \bar{\varepsilon}$, \mathbf{N}_a and $\text{cl}(\bar{\mathbf{N}}_a \setminus \bar{\mathbf{L}}_a)$ are isolating neighborhoods of (1.2) of the invariant set $S = \text{Inv}(\text{cl}(\mathbf{N}_a))$;
- (2) for any $0 < \varepsilon < \bar{\varepsilon}$, the flows on $\mathbf{N}_{\mathbf{R}}$ and $\mathbf{N}_{\mathbf{B}}$ are identical on $\mathbf{E}' := ([-r, r]^2 \times E'_{\mathbf{B}}) \cap \mathbf{N}_{\mathbf{B}}$ for a sufficiently small $r > 0$. See [4, (5.7)] for relevant definitions;
- (3) for any $0 < \varepsilon < \bar{\varepsilon}$,

$$H^*(\bar{\mathbf{N}}_a, \bar{\mathbf{L}}_a) \cong CH^*(S, \varphi^\varepsilon),$$

where φ^ε is the flow of (1.2);

- (4) by Theorem 2.1 the $(2, 1)$ -entry of the transition matrices associated with the boxes $\mathbf{B}_{\mathbf{R}}$, $\mathbf{B}_{\mathbf{B}}$, $\mathbf{B}'_{\mathbf{R}}$, $\mathbf{B}'_{\mathbf{B}}$ are all isomorphisms;

- (5) there are sets $\mathbf{N}_a, \mathbf{L}_a$ such that pairs $(\mathbf{N}_a, \mathbf{L}_a)$ and $(\bar{\mathbf{N}}_a, \bar{\mathbf{L}}_a)$ are homotopically equivalent, and hence $H^*(\mathbf{N}_a, \mathbf{L}_a)$ and $H^*(\bar{\mathbf{N}}_a, \bar{\mathbf{L}}_a)$ are isomorphic.

Given a positive integer J , let σ^J be a finite truncation $\sigma^J = (\sigma_{-J}, \dots, \sigma_J)$ of $\sigma \in \{\mathbf{R}, \mathbf{B}\}^{\mathbb{Z}}$. We construct an index pair corresponding to σ^J as follows.

Let $(\mathbf{N}_a(i), \mathbf{L}_a(i))$ and $(\bar{\mathbf{N}}_a(i), \bar{\mathbf{L}}_a(i))$ be $2J + 1$ copies of these pairs and the flows on them. Define

$$\mathbf{N}^J = \bigcup_{i=-J}^J \mathbf{N}_{\sigma_i}(i) / \sim$$

and

$$\mathbf{L}^J = \bigcup_{i=-J}^J \mathbf{L}_{\sigma_i}(i) / \sim,$$

where \sim is an equivalence relation generated by a natural identification of the flows on $\mathbf{N}_{\sigma_{-j}}(-j)$ and $\mathbf{N}_{\sigma_j}(j)$. Since the flows of the copies of \mathbf{N}_B and \mathbf{N}_R are identical on the corresponding \mathbf{E}' -part, this identification is well-defined. More precisely, letting Σ be a cross section for the flow on \mathbf{E}' given by $v = 0.677$ and $\Sigma(i)$ be the corresponding copies for $\mathbf{N}_a(i)$, we can identify the flows on $E'_{\sigma_j}(j)$ at $\Sigma(j)$ and $\mathbf{B}_{\sigma_{-j}}(-j)$ at $\Sigma(-j)$, hence the flow on \mathbf{N}^J is well-defined and it automatically satisfies the conditions for an isolating neighborhood. Moreover, by the Mayer-Vietoris theorem, we have

$$H^*(\mathbf{N}^J, \mathbf{L}^J) \cong H^*(\mathbf{N}_a, \mathbf{L}_a) \cong H^*(\bar{\mathbf{N}}_a, \bar{\mathbf{L}}_a),$$

which is isomorphic to the Conley index of the basic periodic orbits. Therefore, we can conclude that there exists a periodic orbit $\bar{\psi}_\varepsilon^J$ in \mathbf{N}^J , whose projection goes through E_{σ_i} ($i = -J, \dots, J$) with the prescribed order by σ^J . Observe that the projection of $\bar{\psi}_\varepsilon^J$ to the original (u, v, w, z) -space is a true periodic orbit ψ_ε^J of (1.2).

Let ξ_ε^J be the projection of $\bar{\psi}_\varepsilon^J \cap \Sigma(-1)$, which is an initial point of the periodic orbit ψ_ε^J . Since the collection of the points $\{\xi_\varepsilon^J \mid J = 1, 2, 3, \dots\}$ lies in a compact set $\Sigma \cap \mathbf{N}_{\sigma_0}$, it contains a convergent subsequence, whose limit ξ_ε^σ gives an initial point of the desired orbit satisfying the condition of the theorem. \square

5 Numerics

In this section we describe the numerical computations used in this paper. We performed essentially two kinds of numerical computations: computation of isolating blocks and rigorous computation of trajectories. These are discussed in the next two subsections.

5.1 Rigorous Computation of Trajectories

We compute rigorous approximations for the orbits of (1.5) using the **CAPD Library** [1]. This library uses a Lohner algorithm [9] to compute rigorous enclosures for the solutions of ODEs. Consider the initial value problem

$$\begin{cases} x' = f(x) \\ x(0) = x_0. \end{cases} \quad (5.1)$$

Given a rectangle containing the initial point x_0 and a time step Δt , the basic idea of Lohner algorithm is to numerically integrate (5.1) and return a new rectangle which is guaranteed to contain the solution of (5.1) at time Δt . This process can then be repeated to obtain rigorous enclosures for solutions of (5.1). At each step rigorous error bounds and interval arithmetic are employed to guarantee that the returned rectangle contains the true solution of (5.1). The main difference between the method described above and the algorithms used in the **CAPD Library** is that the latter do not compute a rectangle enclosure for the solution at each step, rather they represent the solution by other types of set (called interval set, doubleton, etc.). This guarantee tighter enclosures and reduces the so called *wrapping effect*. The **CAPD Library** can also compute a rectangle containing the entire trajectory on the time interval $[0, \Delta t]$ (see [13, 12] for further details). The computed trajectories are thus given by a collection of overlapping rectangles, as shown in Figure 9.

Using the **CAPD Library** we computed rigorous enclosures for solutions of (1.5) as shown in Figure 7 and Figure 8. We also computed the unstable manifolds of (1.4) using the **CAPD Library**. To describe how the unstable manifolds were computed, consider the unstable manifold of Figure 5 corresponding to $v = 0.323$ (red curve). We rigorously computed two trajectories using the **CAPD Library** with initial conditions $(0, w^*)$ and $(u^*, 0)$, with $w^* = 4/10000$ and $u^* = 4/10000$, as shown in Figure 10. We then use the fact that $\dot{u} > 0$ on the set $\{(0, w) \mid 0 < w \leq w^*\}$ and $\dot{w} > 0$ on the set $\{(u, 0) \mid 0 < u \leq u^*\}$

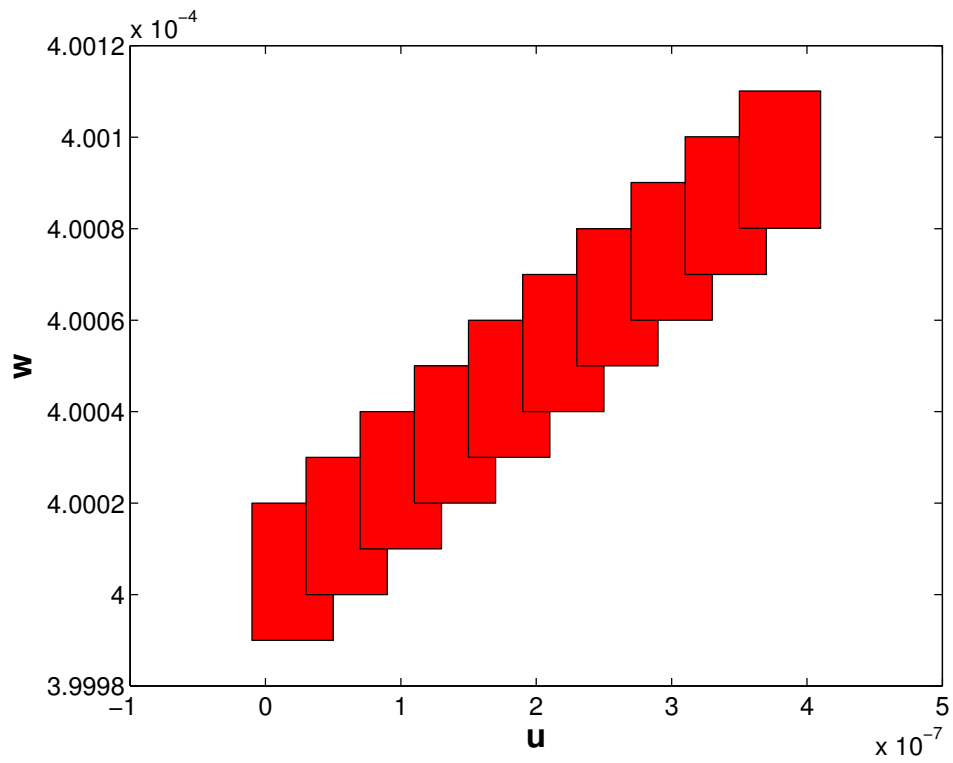


Figure 9: The first ten rectangles representing one of the solutions in Figure 5, computed using the CAPD Library. It is worth mentioning that each solution curve in Figure 5 consists of about 200,000 rectangles.

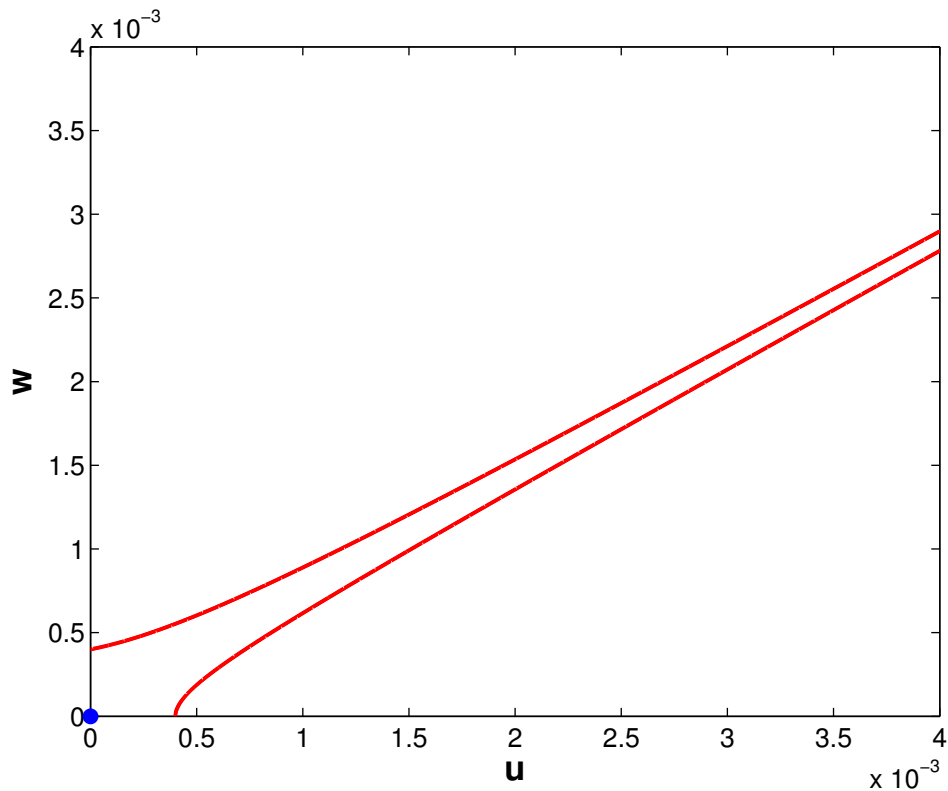


Figure 10: Close-up of Figure 5 near the point $(0, 0)$ showing the two computed solutions which must enclose the unstable manifold for (1.4) with $v = 0.323$.

to conclude that the two red curves in Figure 10 provide outer bounds for the unstable manifold. Therefore notice that the red curve in Figure 5 is in fact formed by two red curves. The other unstable manifolds were computed analogously. The total time for the computation of the unstable manifolds and the trajectories in Figure 7 was 15.5 minutes on a 1.0 GHz P3 machine.

5.2 Computation of Isolating Blocks

In [2], we describe a theoretical foundation for algorithms to compute global qualitative information about the dynamics of flows generated by a system of ordinary differential equations. The main idea is to approximate the dynam-

ics on a compact polygon $\Omega \subset \mathbb{R}^n$ by a multivalued mapping on a polygonal decomposition of Ω . This approximation is determined from the vector field without numerically integrating to approximate specific trajectories. The resulting multivalued map on polygons is a finite, combinatorial representation of the flow from which specific qualitative information can be extracted using topological ideas from the Conley index theory. A general description of such techniques for maps can also be found in [8, 11].

To construct an appropriate polygonal decomposition, we first triangulate Ω by a simplicial complex \mathcal{K} with simplices which are aligned with the flow. Then simplices are aggregated into polygonal regions by removing $(n - 1)$ -faces which are not transverse to the vector field, yielding a polygonal decomposition \mathcal{P} of Ω . This transversality is verified rigorously using interval arithmetic. Thus, on every remaining interior $(n - 1)$ -face the vector field points out of a polygon P and into a polygon Q . The multivalued map $\mathcal{F} : \mathcal{P} \rightrightarrows \mathcal{P}$ is then defined by $Q \subset \mathcal{F}(P)$. The main property of such polygonal decompositions that we will utilize here is stated in the following theorem. For a more detailed description of this construction and properties of such decompositions see [2].

Theorem 5.1 *If \mathcal{Q} is a collection of recurrent polygons in \mathcal{P} and the geometric realization $X = |\cup_{n \geq 0} \mathcal{F}^n(\mathcal{Q})| \cap |\cup_{n \geq 0} \mathcal{F}^{-n}(\mathcal{Q})| \subset \text{int}(\Omega)$, then X is an isolating block for the flow. In particular, if \mathcal{Q} is the set of polygons containing the equilibrium points, then X contains all connecting orbits between equilibria.*

Proof. Follows from the proofs of [2, Theorems 2.18 and 2.20]. □

Now we briefly describe the specific computations performed on the fast system (1.4). First we generate a triangulation in the rectangle $[-0.4, 1.4] \times [-0.7, 0.7]$. The polygonal decomposition resulting from this triangulation is shown in Figure 11. The details of the algorithms used to generate this triangulation are beyond the scope of this brief paper and will be the subject of future work [7]. The polygonal decomposition in Figure 11 was rigorously computed by checking the transversality of each edge for the entire interval of parameter values $v \in [0.275, 0.7]$ using interval arithmetic, then the multivalued map was rigorously constructed. Notice that the multivalued map is valid for all parameter values $v \in [0.275, 0.7]$, since all the edges are transverse for all $v \in [0.275, 0.7]$. Finally the set X was computed starting from

the three polygons containing the three equilibria $(0, 0)$, $(0.3, 0)$, and $(1, 0)$, and so X contains these equilibria as shown in Figure 12. By Theorem 5.1, X is an isolating block for all parameter values $v \in [0.275, 0.7]$. The boundary of the isolating block X has an exit set with two components as shown in Figure 11.

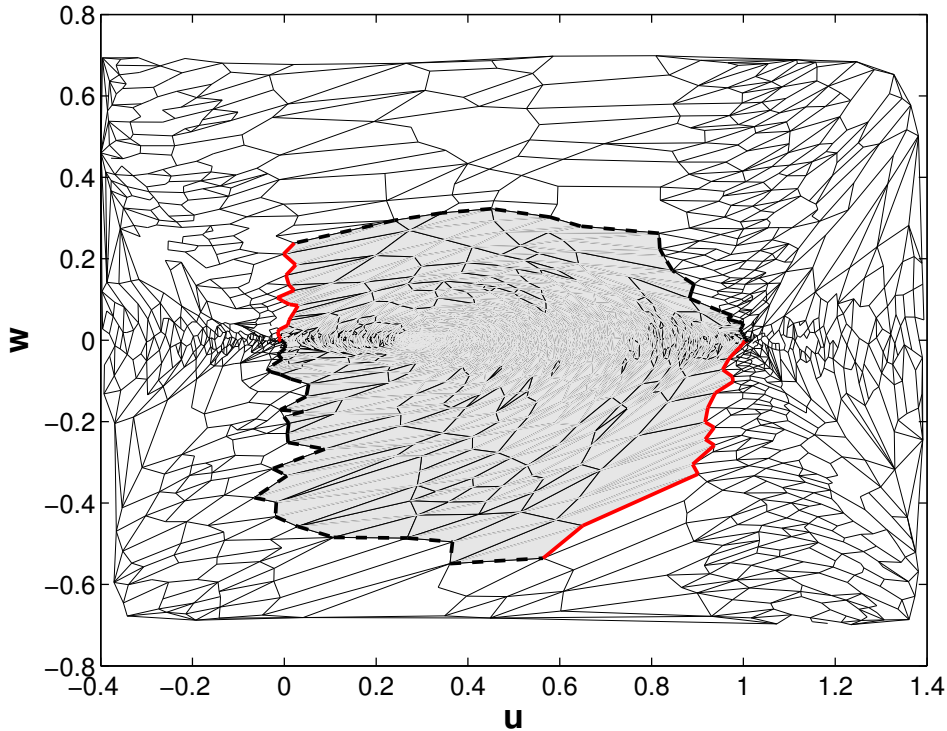


Figure 11: Coarse polygonal decomposition with 2200 vertices and 1308 polygons from 4336 simplices. The gray shaded region is an isolating block X . The black (dashed) portion of ∂X is the immediate exit set, and red (solid) portion is the immediate entrance set.

We should note that the triangulation used is very coarse and only about half of the resulting edges are flow transverse. If a finer triangulation were computed, the number of transverse edges would increase. However, such a finer triangulation, while computable, is not necessary for the results of this paper, which is one of the strengths of the Conley index theory. The total time for these computations, including interval arithmetic, was 2.8 minutes

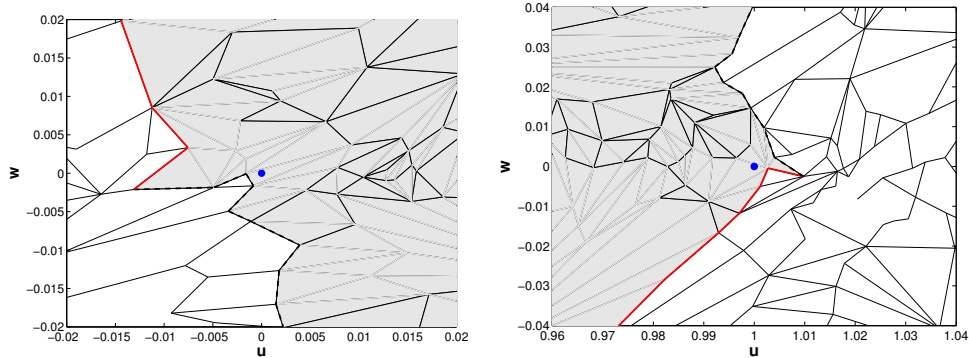


Figure 12: Close-ups of Figure 11 near the fixed points $(0,0)$ and $(1,0)$.

on a 3.0 GHz P4 machine.

Acknowledgements

This work was partially supported by NSF Grant INT-0089631 and by JSPS Japan-U.S. Cooperative Science Program. M. G. was partially supported by NSF grants DMS-0107396, and INT-0089631, DARPA, and CAPES, Brazil. T. G. was partially supported by NSF-BITS grant 0129895, NIH-NCRR grant PR16445 and NSF/NIH grant W0467. W. K. was partially supported by NSF Grant DMS-9973331. H. K. was partially supported by JSPS Grant-in-Aid for Scientific Research (No. 14340055, No. 17340045). K. M. was partially supported by NSF grants DMS-0511115, DMS-0107396, and INT-0089631, and DOE grant 97891, and DARPA. H. O. was partially supported by JSPS Grant-in-Aid for Scientific Research (No. 14540219, No. 17540206). We would like to thank Paweł Pilarczyk for his assistance with the CAPD Library.

References

- [1] CAPD - computer assisted proofs in dynamics group. <http://capd.wsb-nlu.edu.pl/>, 2005.
- [2] E. Boczko, W. D. Kalies, and K. Mischaikow. Polygonal approximation of flows. *Submitted for publication*, 2004.

- [3] R. Gardner and J. Smoller. The existence of periodic travelling waves for singularly perturbed predator-prey equations via the Conley index. *J. Differential Equations*, 47(1):133–161, 1983.
- [4] T. Gedeon, H. Kokubu, K. Mischaikow, and H. Oka. The Conley index for fast-slow systems II: Multi-dimensional slow variable. *Submitted for publication*, 2004.
- [5] C. K. R. T. Jones. Geometric singular perturbation theory. In *Dynamical systems (Montecatini Terme, 1994)*, volume 1609 of *Lecture Notes in Math.*, pages 44–118. Springer, Berlin, 1995.
- [6] C. K. R. T. Jones and A. I. Khibnik, editors. *Multiple-time-scale dynamical systems*, volume 122 of *The IMA Volumes in Mathematics and its Applications*, New York, 2001. Springer-Verlag.
- [7] W. D. Kalies and K. Mischaikow. Algorithms for polygonal approximation of flows. *In preparation*, 2005.
- [8] W. D. Kalies, K. Mischaikow, and R. C. A. M. VanderVorst. An algorithmic approach to chain recurrence. *To appear in Foundations of Computational Mathematics*, 2005.
- [9] R. J. Lohner. Computation of guaranteed enclosures for the solutions of ordinary initial and boundary value problems. In *Computational ordinary differential equations (London, 1989)*, volume 39 of *Inst. Math. Appl. Conf. Ser. New Ser.*, pages 425–435. Oxford Univ. Press, New York, 1992.
- [10] C. K. McCord and K. Mischaikow. Equivalence of topological and singular transition matrices in the Conley index theory. *Michigan Math. J.*, 42(2):387–414, 1995.
- [11] K. Mischaikow. Topological techniques for efficient rigorous computation in dynamics. *Acta Numer.*, 11:435–477, 2002.
- [12] M. Mrozek and P. Zgliczyński. Set arithmetic and the enclosing problem in dynamics. *Ann. Polon. Math.*, 74:237–259, 2000. Dedicated to the memory of Bogdan Ziemian.

- [13] P. Zgliczynski. C^1 Lohner algorithm. *Found. Comput. Math.*, 2(4):429–465, 2002.

(-1.113000e-03,-6.262000e-03)	(3.903000e-03,-9.349000e-03)	(1.798000e-03,-1.266700e-02)
(3.903000e-03,-9.349000e-03)	(1.798000e-03,-1.266700e-02)	(1.477000e-03,-1.704800e-02)
(1.798000e-03,-1.266700e-02)	(1.477000e-03,-1.704800e-02)	(2.240000e-03,-2.011900e-02)
(1.477000e-03,-1.704800e-02)	(2.240000e-03,-2.011900e-02)	(-9.160000e-03,-2.979300e-02)
(2.240000e-03,-2.011900e-02)	(-9.160000e-03,-2.979300e-02)	(-1.341800e-02,-3.672500e-02)
(-9.160000e-03,-2.979300e-02)	(-1.341800e-02,-3.672500e-02)	(-4.725000e-03,-4.644800e-02)
(-1.341800e-02,-3.672500e-02)	(-4.725000e-03,-4.644800e-02)	(-3.834500e-02,-7.005200e-02)
(-4.725000e-03,-4.644800e-02)	(-3.834500e-02,-7.005200e-02)	(-2.925800e-02,-7.789300e-02)
(-3.834500e-02,-7.005200e-02)	(-2.925800e-02,-7.789300e-02)	(-8.797000e-03,-8.419100e-02)
(-2.925800e-02,-7.789300e-02)	(-8.797000e-03,-8.419100e-02)	(1.411700e-02,-9.529300e-02)
(-8.797000e-03,-8.419100e-02)	(1.411700e-02,-9.529300e-02)	(5.296400e-02,-1.079950e-01)
(1.411700e-02,-9.529300e-02)	(5.296400e-02,-1.079950e-01)	(4.768200e-02,-1.383070e-01)
(5.296400e-02,-1.079950e-01)	(4.768200e-02,-1.383070e-01)	(-9.043000e-03,-1.711440e-01)
(4.768200e-02,-1.383070e-01)	(-9.043000e-03,-1.711440e-01)	(4.181000e-02,-1.749900e-01)
(-9.043000e-03,-1.711440e-01)	(4.181000e-02,-1.749900e-01)	(-6.780000e-04,-1.880520e-01)
(4.181000e-02,-1.749900e-01)	(-6.780000e-04,-1.880520e-01)	(9.928000e-03,-2.041890e-01)
(-6.780000e-04,-1.880520e-01)	(9.928000e-03,-2.041890e-01)	(6.938000e-03,-2.294320e-01)
(9.928000e-03,-2.041890e-01)	(6.938000e-03,-2.294320e-01)	(8.109000e-03,-2.511840e-01)
(6.938000e-03,-2.294320e-01)	(8.109000e-03,-2.511840e-01)	(8.824300e-02,-2.673380e-01)
(8.109000e-03,-2.511840e-01)	(8.824300e-02,-2.673380e-01)	(-2.521200e-02,-3.154580e-01)
(8.824300e-02,-2.673380e-01)	(-2.521200e-02,-3.154580e-01)	(6.073000e-03,-3.328580e-01)
(-2.521200e-02,-3.154580e-01)	(6.073000e-03,-3.328580e-01)	(-6.538100e-02,-3.866160e-01)
(6.073000e-03,-3.328580e-01)	(-6.538100e-02,-3.866160e-01)	(-1.745800e-02,-3.981900e-01)
(-6.538100e-02,-3.866160e-01)	(-1.745800e-02,-3.981900e-01)	(-1.935200e-02,-4.333460e-01)
(-1.745800e-02,-3.981900e-01)	(-1.935200e-02,-4.333460e-01)	(2.918400e-02,-4.575130e-01)
(-1.935200e-02,-4.333460e-01)	(2.918400e-02,-4.575130e-01)	(1.073850e-01,-4.844560e-01)
(2.918400e-02,-4.575130e-01)	(1.073850e-01,-4.844560e-01)	(2.676750e-01,-4.859080e-01)
(1.073850e-01,-4.844560e-01)	(2.676750e-01,-4.859080e-01)	(3.664710e-01,-4.954640e-01)
(2.676750e-01,-4.859080e-01)	(3.664710e-01,-4.954640e-01)	(3.611380e-01,-5.487200e-01)
(3.664710e-01,-4.954640e-01)	(3.611380e-01,-5.487200e-01)	(5.637840e-01,-5.353800e-01)
(3.611380e-01,-5.487200e-01)	(5.637840e-01,-5.353800e-01)	(6.500690e-01,-4.557820e-01)
(5.637840e-01,-5.353800e-01)	(6.500690e-01,-4.557820e-01)	(9.013000e-01,-3.288230e-01)
(6.500690e-01,-4.557820e-01)	(9.013000e-01,-3.288230e-01)	(8.895690e-01,-3.050800e-01)

Table 1: List of vertices for the edges forming the boundary of the isolating block X in Figure 4 in order from left to right.